



Close-loop performance of a high precision deflectometry controlled deformable mirror (DCDM) unit for wavefront correction in adaptive optics system

Lei Huang^{a,*}, Chenlu Zhou^a, Wenchuan Zhao^b, Heejoo Choi^c, Logan Graves^c, Daewook Kim^c

^a Department of Precision Instruments, Tsinghua University, Beijing 100084, China

^b Chinese Academy of Sciences, The Institute of Optics and Electronics, Chengdu 610209, China

^c College of Optical Sciences, University of Arizona, 1630 East University Boulevard, Tucson, AZ 85721, USA

ARTICLE INFO

Keywords:

Adaptive optics
Deformable mirror
Wavefront
Deflectometry
High power laser

ABSTRACT

We present a high precision deflectometry system (DS) controlled deformable mirror (DM) solution for optical system. Different from wavefront and non-wavefront system, the DS and the DM are set to be an individual integrated DCDM unit and can be installed in one base plate. In the DCDM unit, the DS can directly provide the influence functions and surface shape of the DM to the industrial computer in any adaptive optics system. As an integrated adaptive unit, the DCDM unit could be put into various optical systems to realize aberration compensation. In this paper, the configuration and principle of the DCDM unit is introduced first. Theoretical simulation on the close-loop performance of the DCDM unit is carried out. Finally, a verification experiment is proposed to verify the compensation capability of the DCDM unit.

1. Introduction

With the remarkable development of adaptive optics, deformable mirror (DM) is applied widely to compensate aberration in optical system, including imaging optical system, laser system and astronomical instrumentation. In order to achieve high precision aberration compensation, two typical kinds of sensors, i.e. wavefront sensor and non-wavefront sensor, have been widely used to acquire the aberration in optical system.

An infrared CCD camera as non-wavefront sensor and a 32 mm aperture 19-element piezoelectric DM are used to detect and correct the distortion of output laser beam [1]. A single point defocus DM creating a large-area convex, based on a Hartmann wavefront sensor, are used to compensate the wavefront aberration in a Nd: YAG rod amplifier [2]. In another application, a Shack-Hartmann wavefront sensor and a 82 mm aperture 64-element piezoelectric DM are applied to improve the beam quality of fiber laser [3]. A Shack-Hartmann sensor, a thermally actuated DM and a membrane DM are used to predictive control the thermally induced wavefront aberrations [4]. In other aberration correction applications, Shack-Hartmann sensor is also widely used to achieve wavefront sensing [5–8]. A 15 mm diameter 37-hexagonal-actuator membrane DM and a silicon photodiode non-wavefront sensor are presented to realize intracavity correction in a Nd:

YVO₄ solid-state laser [9]. Especially, in this application [9], an additional Michelson interferometer is constructed to monitor the mirror shaping changing of the DM. In wavefront sensor applications, the DM influence functions and system wavefront aberration are measured by wavefront sensor. Close-loop algorithm based on the DM influence functions enables the real time correction of system wavefront aberration. As a typical wavefront sensor, Shack-Hartmann sensor has shown high speed and high efficiency in low order aberration correction.

However, in the application of high slopes and strong deviations correction, Shack-Hartmann sensor is not much suitable. The low-resolution sensor could not precisely acquire the aberration. The high-resolution sensor is restricted for the limited dynamic range, and only applicable to high precision wavefront acquisition. In non-wavefront sensor applications, without any wavefront acquisition, aberration close-loop correction is mainly ensured by SPGD algorithm [1,3,9,10]. However, the global optimum is always a big challenge for non-wavefront correction in various optical systems. Additional wavefront sensor is always chosen to be an essential accessory in non-wavefront sensor adaptive optics system.

In this paper, we present a high precision deflectometry system (DS) [11,12] controlled DM solution for optical system. Different from wavefront and non-wavefront system, the DS and the DM is set to be an

* Corresponding author.

E-mail address: hl@tsinghua.edu.cn (L. Huang).

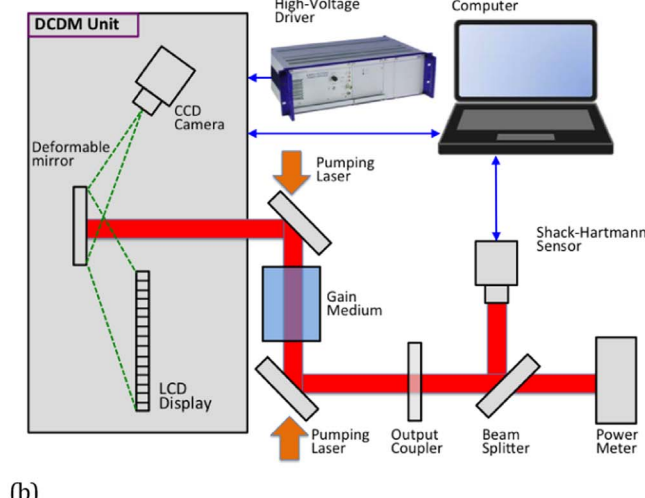
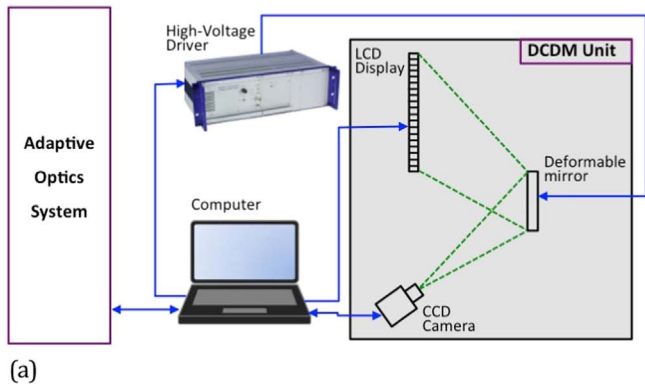


Fig. 1. The layout of DCDM unit (a), and an applicable adaptive optics system (b).

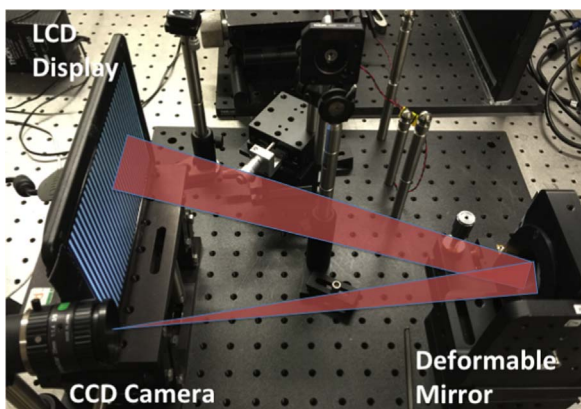


Fig. 2. The DCDM unit realized in the laboratory.

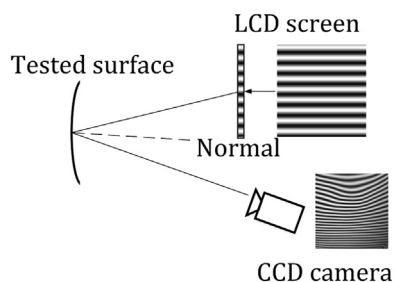


Fig. 3. Configuration of the deflectometry measurement system.

individual integrated unit and installed in one base plate, called DCDM (i.e. Deflectometry Controlled DM). In the DCDM unit, the DS can directly provide the influence functions and surface shape of the DM to the industrial computer. Note that the DM's surface, not its wavefront, is directly measured by the DS in the presented DCDM configuration. Unlike other wavefront sensor applications (e.g. Shack–Hartmann sensor) measuring the wavefront at a limited spatial resolution (e.g., 20×20 lenslet array), acquiring a high-resolution DM surface map (e.g., 500×500 pixels) is essential for decreasing the data acquisition error. As an integrated adaptive unit, the high DCDM unit could be put into various optical systems to realize aberration compensation. In this paper, the configuration and principle of the DCDM unit is introduced first. Theoretical simulation on the close-loop performance of the DCDM unit is carried out. Finally, a verification experiment is proposed to verify the validation of the DCDM unit.

2. Configuration and principle

Fig. 1 describes the layout of the DCDM unit (Fig. 1(a)) and an applicable adaptive optics system (Fig. 1(b)).

In the layout of the DCDM unit, it mainly consists of a high precision DS (a LCD display and a CCD camera), a DM and an industrial computer. Different from wavefront and non-wavefront system, the DCDM is set to be an individual integrated unit (Fig. 1(a)) and installed in one base plate. Three interfaces are set to connect the DCDM unit to the power and control unit, i.e. the driving interface of DM to the high-voltage driver, the data interfaces of LCD display and CCD camera to the industrial computer. While working, the raw measurement data of surface shape of the DM are sent to the industrial computer, through the data interface between CCD camera and computer. After data processing, influence functions and DM surface shape are stored. Target compensation aberration is calculated in computer based on the data from adaptive optics system and the stored DM surface shape. In close-loop operation, the DM is driven by the high-voltage driver according to the command from computer to achieve aberration compensation.

An applicable adaptive optics system in high power laser is demonstrated in Fig. 1(b). It mainly consists of a laser oscillator, a high precision DCDM unit, a high-resolution Shack-Hartmann sensor (SHS), and an industrial computer. In this system, the measurement and control accuracy is mostly determined by the precision of the SHS and the DCDM. The DCDM unit, as an individual integrated unit, provides raw data of influence functions and DM surface shape to the computer. Also, the DS in the DCDM must be calibrated before measurement. The high-resolution SHS ensures the accurate measurement on the system wavefront. In order to decrease the effect of system aberration, the original aberration acquired by SHS is saved as a background in computer.

In the following part of this paper, we will focus on the basic performance and close-loop control reliability of the DCDM unit (Fig. 1(a)). In our future research, an applicable adaptive optics in laser system using the DCDM unit will be studied and reported.

An actual DCDM unit was designed and built as shown in Fig. 2. A LCD display (Mimo Inc., UM-710S, 7", 800*480) and a CCD camera (PointGrey Inc., Flea3 1.3 MP Mono USB3 Vision, VITA 1300) were used to build the DS. A membrane DM (ALPAO Inc., DM52-25, pupil diameter 15 mm, 52-actuator, wavefront 3*3 stroke 15 μm) was measured and controlled by the DS. Note that the DS's size could be set as small as twice of the DM's size, according to the principle of ray tracing. Based on this, a more compact configuration of the DCDM could be achieved in practical AO system (e.g. A 2.4" compact LCD display and a 29 mm*29 mm*30 mm PointGrey CCD camera could be used to match the 15 mm aperture DM).

It was described in [13–16] that the surface could be precisely measured based on the deflectometry method (Fig. 3). According to the detailed analysis in [13], the surface slopes can be calculated by acquiring

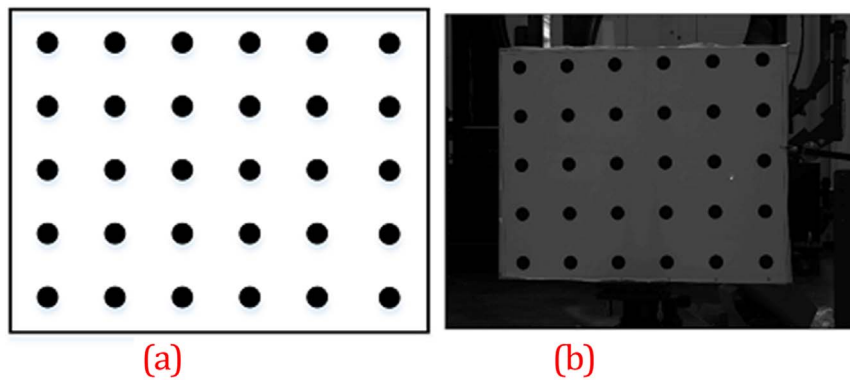


Fig. 4. The reference screen with standard dots pattern (a) and its image in the CCD camera (b).

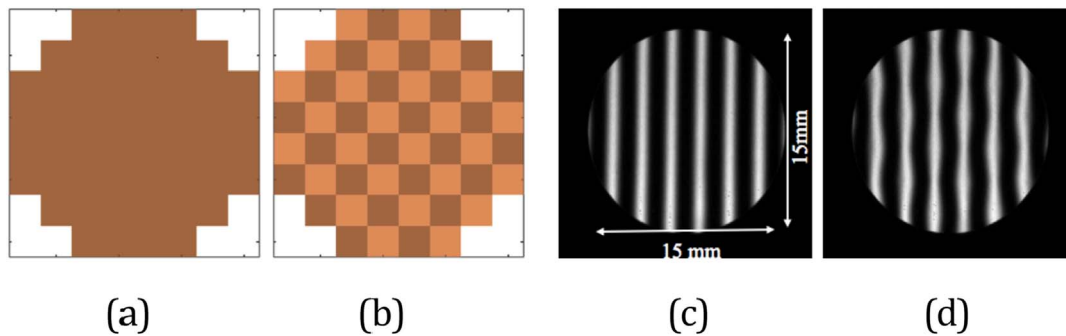


Fig. 5. Relationship between the layout of the DM driven actuators and deflectometry fringe patterns measured in the DS camera. (c) is the original fringe without surface shape deformation (a). (d) is the deformed fringe for deformation (b). The brown and orange areas in (b) represent 52 actuators of the DM.

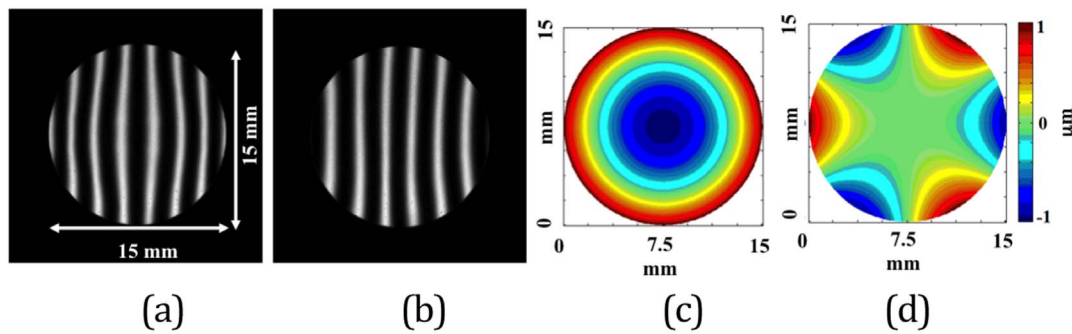


Fig. 6. Relationship between the generated wavefront in DM and deflectometry fringe patterns measured in the DS camera. (a) is the deformed fringe due to the 4th term Zernike mode (c) in DM. (b) is the deformed fringe due to 9th term Zernike shape (d) in DM.

the locations of the lit pixel on the LCD display, the CCD camera and the mirror bright region (Eq. (1) in [13]). By phase shifting of the fringe pattern and images taken by CCD camera, x and y slopes of tested surface could be calculated as Eqs. (1) and (2) (Eqs. (1) and (2) in [14,15]).

$$\frac{\partial W(x, y)}{\partial x} \cong -\frac{\Delta x_{screen}}{d_{m2screen}}, \quad \frac{\partial W(x, y)}{\partial y} \cong -\frac{\Delta y_{screen}}{d_{m2screen}} \quad (1)$$

$$\Delta x_{screen} = x_{measured} - x_{ideal}, \quad \Delta y_{screen} = y_{measured} - y_{ideal} \quad (2)$$

Where $W(x,y)$ is the wavefront aberration, x and y are the coordinates of the LCD screen pixel, $d_{m2screen}$ is the measured distance from LCD screen to tested surface. When the slopes are measured, it can be integrated using a polynomial fit to the slopes or by zonal integration methods to give the surface shape [13].

The precision of the DS mostly determines the accuracy of DCDM unit. In order to achieve high accuracy, the DS in the DCDM must be calibrated before measurement. First, a reference screen with standard dots pattern is placed into the system exactly at the same position of the DM and its image is detected by the CCD camera (Fig. 4). In this

process, systematic error (e.g. distortion of the camera) could be calibrated with the dots pattern and its image in CCD camera. The distance of two dots on screen is precisely controlled. Correspondence relationship between CCD coordinate system and DM coordinate system could be built up with measured result. A standard reference flat mirror is then placed at the same position of the DM and measured by the DS. The measurement result is applied as a standard reference plane, which will be taken as the calibrated background [17,18]. After the one time calibration during the system build-up stage, the DS could achieve precision as high as 1 nm [14] and the DCDM unit could reach high precision. After DS calibration, the whole DCDM unit is built up.

In Fig. 5, according to the principle of deflectometry, the deformation of deflectometry fringe patterns has unique relationship with the surface shape of the DM. The measurement demonstration is shown in Fig. 5, which provides the fringes comparison in the DS. Fig. 5(a), (b) indicate the layout of the driven actuators in DM, while Fig. 5(c), (d) provide the comparison of fringes deformation in the camera of DS. As additional information, two measurement data of the DS is presented in Fig. 6, which describes the deformation of deflectometry fringe

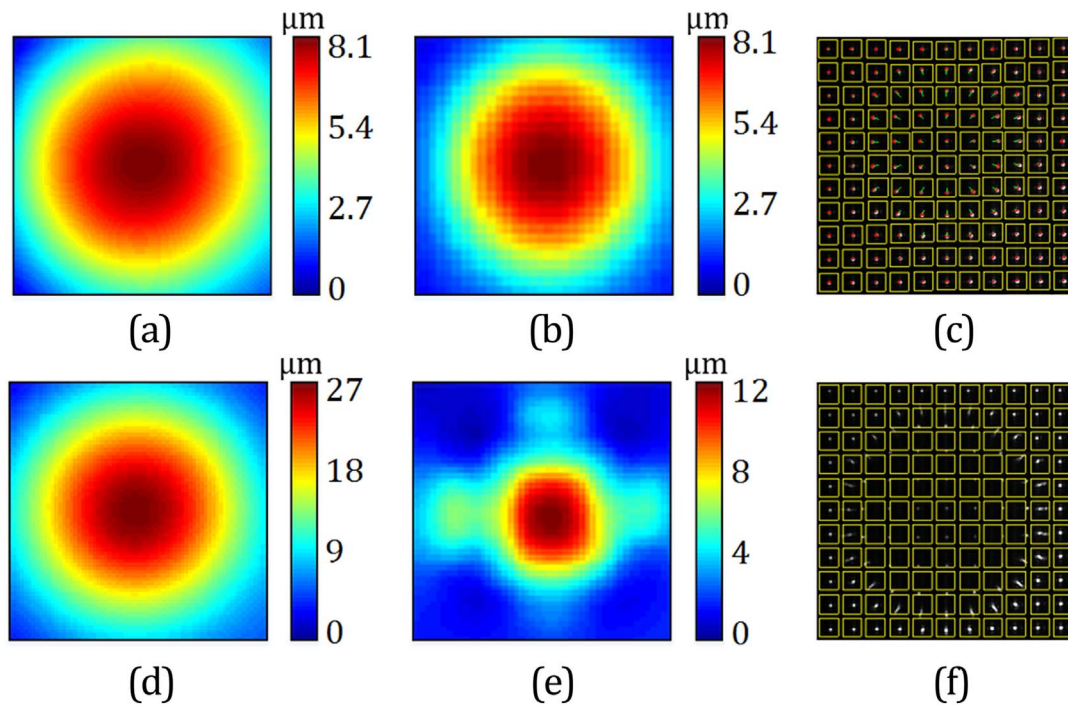


Fig. 7. The small deformation DM measured by DS (a) and SHS (b) (spots array (c)) when 30 V driven voltage applied, while the large deformation DM measured by DS (d) and SHS (e) (spots array (f)) when 90 V driven voltage applied.

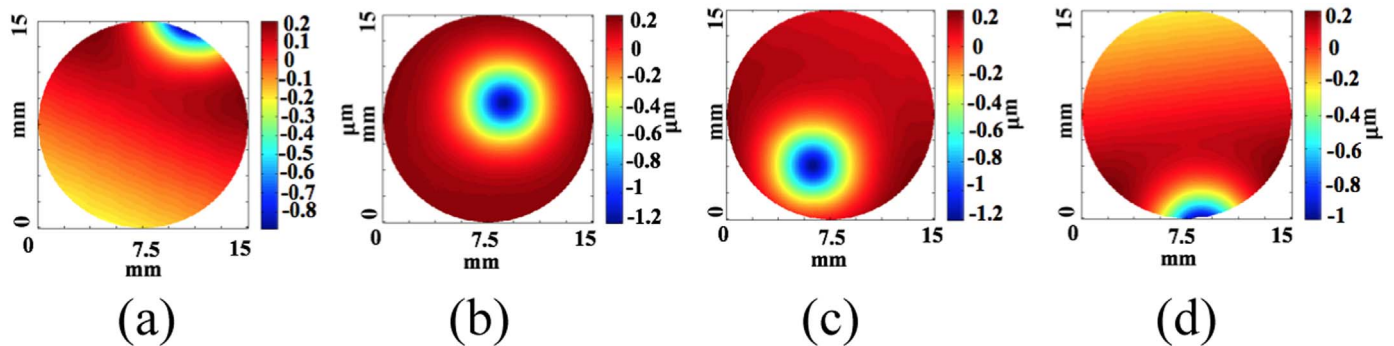


Fig. 8. Measured influence functions. No.1 (a), No.22 (b), No. 39(d), No.50 (d) actuators.

patterns in the DS camera image Fig. 6(a), (b) for two example Zernike modes DM surface shapes in Fig. 6(c), (d).

A comparative experiment is carried out to test the performance of DS and wavefront sensor. A single-actuator DM is used in the experiment and measured by DS and SHS when it is driven with 30 V and 90 V voltage. Fig. 7 shows the measurement results. As we could see, when the testing DM is driven with 30 V voltage, the DS and SHS could both detect the small deformation (Fig. 7(a) and (b), PV 8.1 μm), while the DS could provide much more high resolution. When the DM is driven with 90 V voltage, the DS could still accurately measured the large deformation of DM (Fig. 7(d), PV 27 μm), while it exceeds the SHS's dynamic range.

3. Analysis and experiment results

In the DCDM unit, three aspects of factors affect the reliable surface control of DM, including the measurement accuracy of the mirror surface shape, the deformation ability of DM surface controlled by the DS, the closed-loop precision of the integrated unit. According to the simulation and control principle of the DM, the deformable ability is determined by the influence functions, while the close-loop precision depends on the combination of the DM and the DS.

As we know, the measurement principle of the DS is pixel response, which uses phase shifting methods for data acquisition. The precision of the DS is not restricted by the size of sub apertures as in SHS method. This means it is possible for the DS to measure real influence functions under high stroke, which will eventually decrease acquisition error caused by nonlinear interpolation. One of the challenges is how to coordinate the sampling pixels to make the close-loop in both high precision and high speed.

In our experiment, the influence functions of the DM are measured at 10% percent of the maximum stroke for each actuator and shown in Fig. 8 (Influence functions for typical four actuators). In actual operation, the influence functions, only determined by the variation of the surface shapes, will be the subtraction of the surface shapes before and after deformation. The measurement of influence functions could be carried out after the system calibration of the DCDM unit.

Based on the measured influence functions, in order to achieve the compensation wavefront aberration in adaptive optics system, a gradually fitting algorithm will be carried out to realize closed-loop control. When the process comes to the end, a final surface shape S_e generated by the DM will be very close to the compensation wavefront aberration S_t (Eqs. (3) and (4)).

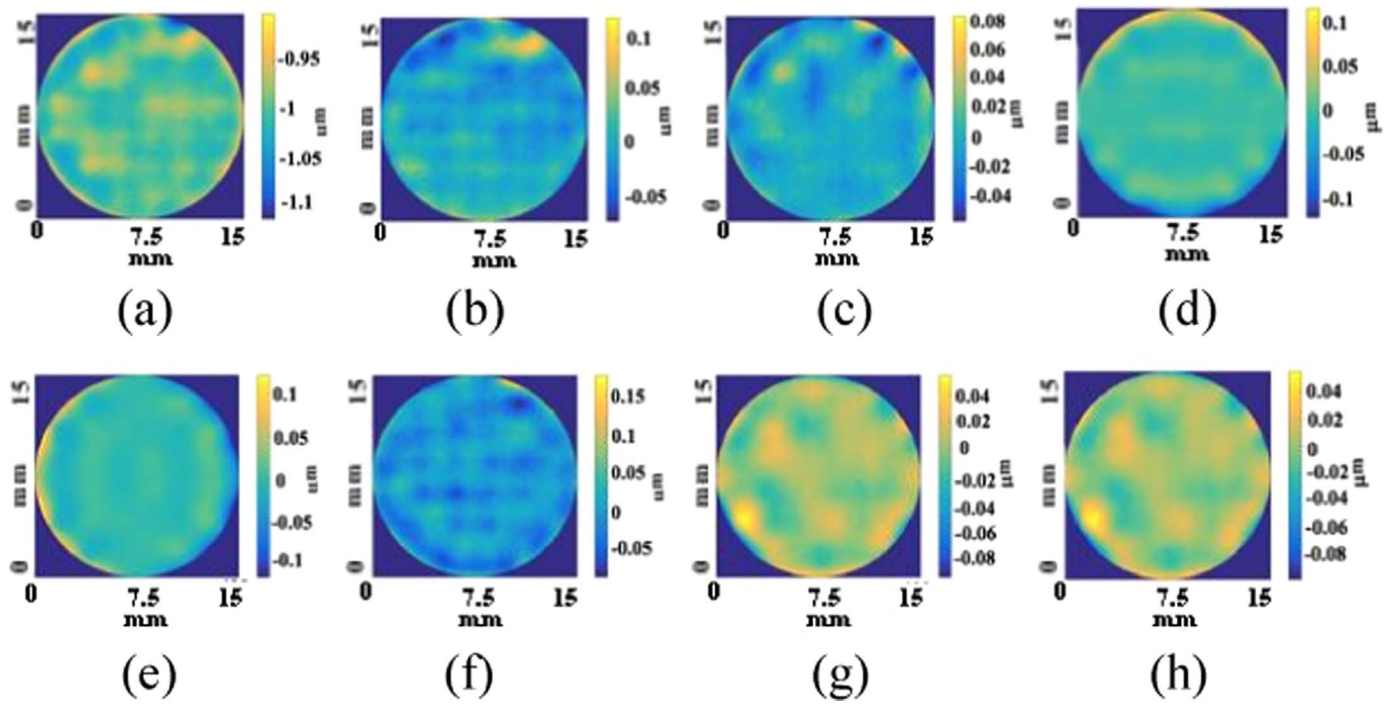


Fig. 9. Simulation results of 4th–11th term Zernike mode (μm), detailed data listed in Table 1 ((a)–4rd, (b)–5th, (c)–6th, (d)–7th, (b)–8th, (b)–9th, (b)–10th, (b)–11th).

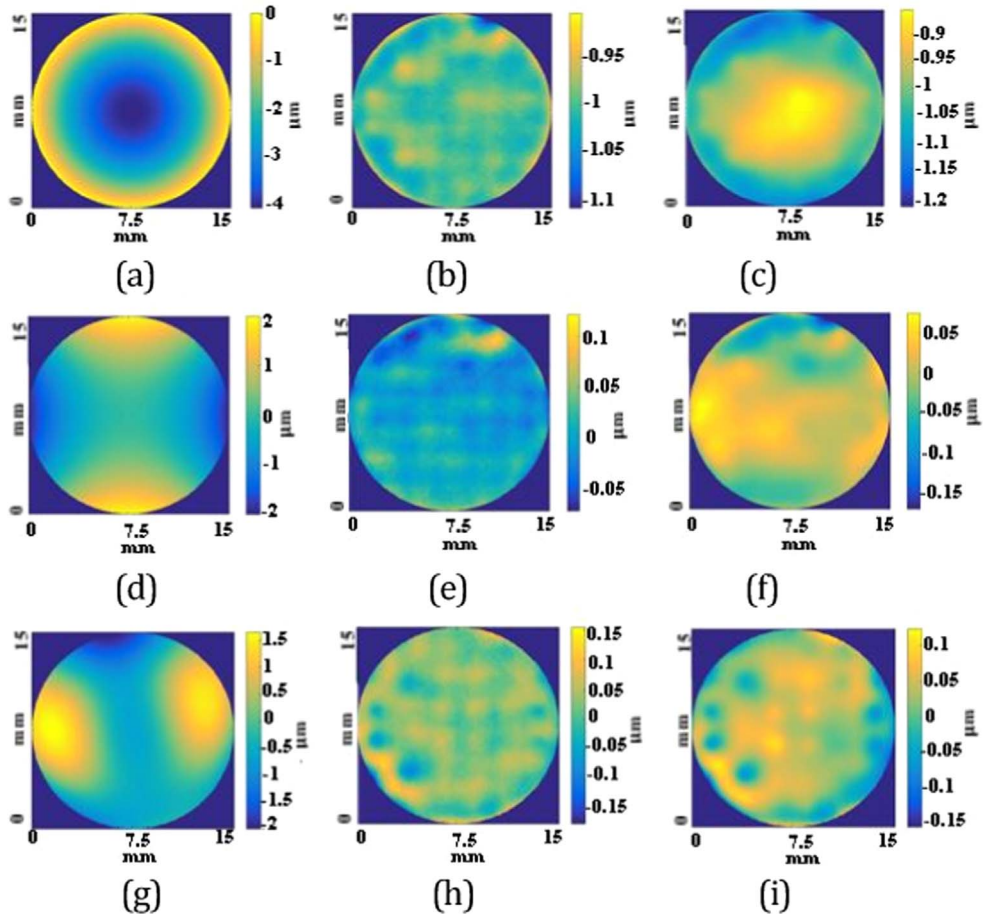


Fig. 10. Experiment results for surface fitting (μm). Desired surface shapes of 4th (PV=4 μm), 5th (PV=4 μm) and random aberration (PV=3.5 μm) are shown in (a), (d) and (g). In simulation, PV/RMS value decrease to 0.221 μm /0.035 μm (b), 0.196 μm /0.022 μm (e) and 0.309 μm /0.027 μm (h) for 4th (a), 5th (d) and random aberration (g), while in experiment, PV/RMS value decrease to 0.363 μm /0.070 μm (c), 0.244 μm /0.032 μm (f) and 0.286 μm /0.021 μm (i) accordingly.

Table 1
Simulation (after s) and experiment (after e) results of surface fitting (μm).

Zernike mode	4	5	6	7	8	9	10	11
PV (before)	4.000	4.000	4.000	4.000	4.000	4.000	4.000	4.000
PV (after s)	0.221	0.196	0.141	0.249	0.256	0.284	0.143	0.155
PV (after e)	0.363	0.244	0.259	0.430	0.452	0.412	0.285	0.286
RMS (before)	1.147	0.817	0.815	1.060	1.060	1.192	0.706	0.707
RMS (after s)	0.035	0.022	0.014	0.039	0.040	0.027	0.026	0.026
RMS (after e)	0.040	0.032	0.047	0.062	0.071	0.045	0.047	0.037

Table 2
Experiment results of surface fitting for large desired compensation aberration (μm).

Zernike mode	4	5	6	7	8
PV=10.061	PV=0.583 RMS=0.054	PV=0.472 RMS=0.048	PV=0.454 RMS=0.051	PV=0.658 RMS=0.072	PV=0.693
PV=20.122	PV=1.159 RMS=0.105	PV=1.089 RMS=0.097	PV=1.078 RMS=0.102	PV=1.345 RMS=0.122	PV=1.425 RMS=0.161

$$S_e = \sum V_i I_i \quad (3)$$

$$\Delta S_e = S_e - S_t \quad (4)$$

Here, I_i are influence functions; V_i is voltage of each actuator; S_t is the desired compensation wavefront aberration; S_e is the final generated surface shape; the fitting residual ΔS_e represents the precision of surface shape fitting.

The surface shape fitting precision greatly influences the application of the DCDM unit, as it will determine the compensation ability and the dynamic range of our system. In order to analyze the compensation precision of the DCDM unit, detailed analysis is primarily carried out in simulation and experiment.

As any aberration could be considered of the combination of Zernike modes, typically from 4th to 11th term (defocus, astigmatism, coma), we demonstrated the simulation from 4th term up to 11th term Zernike mode to examine the compensation ability of the DCDM unit. The simulation residuals for Zernike mode are displayed in Fig. 9–Fig. 10 and Table 1–Table 2.

From the simulation and experiment results shown in Fig. 9–Fig. 10 and Table 1–Table 2, the DCDM unit built in the lab has good capability to generate the fitting surface to compensate the wavefront aberration in adaptive optics system. From the simulation results for 4th–11th order Zernike modes in Fig. 9 and Table 1, the fitting residual PV is less than $0.3 \mu\text{m}$ from original $4 \mu\text{m}$ and RMS less than 40 nm . The experiment results in Table 1 verify the accuracy of the simulation. From the data listed in Table 2, we could figure out that the fitting ability for our DCDM unit is high enough (residual PV less than $0.7 \mu\text{m}$ from $10 \mu\text{m}$, less than $1.5 \mu\text{m}$ from $20 \mu\text{m}$) to compensate the desired aberration with small residual. Fig. 10 demonstrates the experiment results for the compensation of 4th, 5th and random aberration. The simulation results are very close to the experiment results. In simulation, PV/RMS value decrease to $0.221 \mu\text{m}/0.035 \mu\text{m}$, $0.196 \mu\text{m}/0.022 \mu\text{m}$ and $0.309 \mu\text{m}/0.027 \mu\text{m}$ for 4th, 5th and random aberration separately, while in experiment, PV/RMS value decrease to $0.363 \mu\text{m}/0.070 \mu\text{m}$, $0.244 \mu\text{m}/0.032 \mu\text{m}$ and $0.286 \mu\text{m}/0.021 \mu\text{m}$.

4. Discussion and conclusion

From the experiment data, it is important to choose a proper DM in the DCDM unit, considering the actuators layout, clear aperture and maximum stroke, to fit the desired wavefront aberration. Another important parameter of the DCDM unit is the close-loop processing time. In the present DCDM experiment setup, the measurement time of surface is 16 s using multi-images acquisition technology, and it costs around 100 s to complete a close-loop process. However, the surface measure-

ment time will be greatly improved after adopting one-image acquisition technology in our optimized DCDM unit according to the next research plan. In the one-image acquisition technology, when the DS is precisely calibrated, a two-dimensional fringe pattern could be used to replace the one-dimensional fringe pattern. Fourier transform is applied instead of phase shift, and we could obtain both x and y slope at one time. The surface to be measured could be reconstructed with one image.

In this paper, we presented a high precision DCDM solution for adaptive optics system. The DCDM unit consist of a high precision DS and a DM. In the integrated unit, the DS can directly provide the influence

functions and surface shape of the DM to the industrial computer in adaptive optics system. The configuration and principle of the DCDM unit is introduced, and theoretical simulation on the close-loop performance of the DCDM unit is also carried out. Finally, a verification experiment is proposed to investigate the close-loop performance of the DCDM unit. From the simulation and experiment results, the DCDM unit built in the lab has good capability to generate the fitting surface to compensate the wavefront aberration in adaptive optics system. In our next research, the DCDM unit will be put into a typical solid-state laser system to achieve the real-time aberration compensation.

References

- [1] P. Yang, M. Ao, Y. Liu, B. Xu, W. Jiang, Intracavity transverse modes controlled by a genetic algorithm based on Zernike mode coefficients, *Opt. Express* 15 (2007) 17051.
- [2] J. Schwarz, M. Ramsey, D. Headley, P. Rambo, I. Smith, J. Porter, Thermal lens compensation by convex deformation of a flat mirror with variable annular force, *Appl. Phys. B* 82 (2006) 275–281.
- [3] Q. Bian, L. Huang, X. Wang, X. Ma, P. Yan, M. Gong, Experimental investigation on the beam quality improvement of the fiber laser by adaptive optics, *Laser Phys.* 25 (2015) 125101.
- [4] W. Lubeigt, G. Valentine, J. Girkin, E. Bente, D. Burns, Active transverse mode control and optimization of an all-solid-state laser using an intracavity adaptive-optic mirror, *Opt. Express* 10 (2002) 550.
- [5] M. Rais, J. Morel, C. Thiebaut, J. Delvit, A. Facciolor, Improving wavefront sensing with a Shack-Hartmann device, *Appl. Opt.* 55 (2016) 7836–7846.
- [6] Lei Huang, Xingkun Ma, Mali Gong, Qi Bian, Experimental investigation of the deformable mirror with bidirectional thermal actuators, *Opt. Express* 23 (2015) 17520.
- [7] Clélia Robert, Vincent Michau, Bruno Fleury, Serge Magli, Laurent Vial, Mid-infrared Shack-Hartmann wavefront sensor fully cryogenic using extended source for endoatmospheric applications, *Opt. Express* 20 (2012) 15636.
- [8] Jim Schwiegerling, Edward DeHoog, Problems testing diffractive intraocular lenses with Shack-Hartmann sensors, *Appl. Opt.* 49 (2010) D62.
- [9] A. Haber, A. Polo, I. Maj, S.F. Pereira, H.P. Urbach, M. Verhaegen, Predictive control of the thermally induced wavefront aberrations, *Opt. Express* 21 (2013) 21530.
- [10] Brenton James Polans, Oscar M. Keller, Francesco Carrasco-Zevallos, LaRocca, Elijah Cole, Heather E. Whitson, Eleonora M. Lad, Sina Farsiu and Joseph A. Izatt, “wide-field retinal optical coherence tomography with wavefront sensorless adaptive optics for enhanced imaging of targeted regions”, *Biomed. Opt. Express* 8 (2017) 16.
- [11] J.H. Burge, P. Su, G. Butel, R. Huang, A. Maldonado, Measuring large mirrors using SCOTS: the Software Configurable Optical Test System, *Proc. SPIE*, **9151**, 91510Z1–13 (2014).
- [12] T. Zhou, K. Chen, H.Y. Wei, Y. Li, 3D shape reconstruction of specular surfaces by using phase measuring deflectometry, *Proc. SPIE*, **10155** (2016).
- [13] P. Su, R.E. Parks, L. Wang, R.P. Angel, J.H. Burge, Software configurable optical test system: a computerized reverse Hartmann test, *Appl. Opt.* 49 (2010) 4404–4412.
- [14] R. Huang, P. Su, J.H. Burge, L. Huang, M. Idir, High-accuracy aspheric x-ray mirror metrology using software configurable optical test System/deflectometry, *Opt. Eng.* 54 (2015) 084103.
- [15] R. Huang, P. Su, J. H. Burge, M. Idir, X-ray mirror metrology using SCOTS/deflectometry, *Proc. SPIE*, **8848**, 88480G1–6 (2013).
- [16] T. Zhou, K. Chen, H.Y. Wei, Y. Li, Improved method for rapid shape recovery of large specular surfaces based on phase measuring deflectometry, *Appl. Opt.* 55 (2016) 2760.
- [17] R. Huang, P. Su, J.H. Burge, Optical metrology of a large deformable aspherical mirror using software configurable optical test system, *Opt. Eng.* 53 (2014) 085106.
- [18] H.Y. Ren, F. Gao, X.Q. Jiang, Iterative optimization calibration method for stereo deflectometry, *Opt. Express* 23 (2015) 22060–22068.